Sedimentary Geology 223 (2010) 150–161

Contents lists available at ScienceDirect

Sedimentary Geology

journal homepage: www.elsevier.com/locate/sedgeo

Meteoric lithification of catastrophic rockslide deposits: Diagenesis and significance

Diethard Sanders [a,*], Marc Ostermann [a], Rainer Brandner [a], Christoph Prager [b]

[a] Institute of Geology and Palaeontology, Faculty of Geo- and Atmospheric Sciences, University of Innsbruck, Innrain 52, A-6020 Innsbruck, Austria
[b] alpS Natural Hazard Management, Grabenweg 3, A-6020 Innsbruck, Austria

ARTICLE INFO

Article history:
Received 26 May 2009
Received in revised form 9 November 2009
Accepted 11 November 2009

Keywords:
Mass-wasting
Rockslides
Landslides
Meteoric diagenesis
Meteoric cementation

ABSTRACT

Deposits of catastrophic rockslides composed of lithologies rich in carbonate minerals may undergo precipitation of cements that can be used to proxy-date the rockslide event and/or subsequent geomorphic changes of the rockslide mass.

In the Alps, localized to widespread lithification of post-Glacial rockslide deposits is observed in lithologies ranging from limestones and dolostones to metacarbonates to calcphyllites. Lithification of rockslide deposits to breccias may be localized to meteoric 'runoff-shadows' below larger boulders, or may comprise a layer of breccia or may affect a rockslide mass down its base. In addition, precipitation of cements and small stalactites may take place in megapores on boulder undersides. Cements found in rockslide deposits comprise skalenohedral calcite, prismatic calcite, blocky calcite, calcitic micrite and micropeloidal calcitic cement and, rarely, botryoidal aragonite. Initial cement formation probably is driven by meteoric dissolution–re-precipitation of (mini-) micritic abrasive rock powder generated by dynamic disintegration during the rockslide event. Preliminary $^{234}U/^{230}Th$ ages of rockslide cements support a concept that cementation starts immediately or early after a rockslide event. In rockslide deposits of calcphyllite with accessory pyrite, oxidation of pyrite probably also propels the process of carbonate dissolution–re-precipitation. Limestone-precipitating springs emerging from rockslide masses, and well-cemented talus slopes and fluvial conglomerates percolated by rockslide-derived groundwaters, indicate that rockslide deposits remain diagenetically active long after emplacement.

1. Introduction

Catastrophic rockslides are gravity-driven, rapid mass movements with volumes of more than 10^5 m^3 (Evans et al., 2006). According to Evans et al. (2006), these may be subdivided into (a) rockslides *s. str.*, if the downslope travel distance is limited, disintegration of the slide mass incomplete, and if a significant portion of the slide mass rests on the initial detachment surface, and (b) rock avalanches or sturzstroms (cf. Hsü, 1975) if the rock mass is more-or-less completely disintegrated into boulders to cataclastic gouge, and had entirely passed-by its initial detachment surface upon rapid downslope movement. Although they are rare events to human perception, catastrophic rockslides are geologically frequent and normal processes of orogenic erosion and mass balance (Gilchrist et al., 1994; Ballantyne, 2002; Hovius and Stark, 2006). Rockslides have been intensely investigated from different perspectives such as the style of mass movement, risk prediction, age-dating of events, and their potential relation with earthquakes and climate (Heim, 1932; Eisbacher and Clague, 1984; Erismann and Abele, 2001; Kilburn and Pasuto, 2003). To assess the hazard of future rockslide events, age-dating of previous rockslides is a crucial prerequisite (Prager et al., 2008; Ivy-Ochs et al., 2009). For the Eastern Alps, spatio-temporal clusters in post-Glacial rockslide activity are indicated, yet a straight correlation with climatic changes and/or with earthquake frequency to date seems elusive (Prager et al., 2008).

An aspect hitherto overlooked is that rockslide deposits composed of lithologies rich in carbonate minerals may undergo localized to, probably, wholesale lithification in a meteoric diagenetic environment. Aside from rare cursory mention in previous literature (Abele, 1974; Weidinger, 1998), rockslide lithification to date was not systematically explored. In addition, $^{234}U/^{230}Th$ dating of meteoric cements in rockslide deposits can provide a good proxy age of the mass-wasting event (Ostermann et al., 2007; Prager et al., 2009). The present investigation of seven rockslides of the Alps (Fig. 1) describes and interprets the patterns of lithification. The significance of meteoric diagenetic cements for U/Th age-dating is briefly discussed. We suggest that lithification indeed is common in carbonate-lithic rockslide deposits. The rockslides described herein are from most of the major tectonic units of the Alps, and comprise non-metamorphic carbonate rocks, metacarbonates, marbles, and calcareous phyllites (Fig. 1, Table 1).

* Corresponding author.
E-mail address: Diethard.G.Sanders@uibk.ac.at (D. Sanders).

0037-0738/$ – see front matter © 2009 Elsevier B.V. All rights reserved.
doi:10.1016/j.sedgeo.2009.11.007

2. Methods

The rockslide deposits described herein were inspected and sampled in the field. Each of the investigated rockslide masses today is largely covered by forest mainly of *Pinus sylvestris*, *Picea abies* and, subordinately or locally, of *Larix decidua* and *Abies alba*. Field sampling of diagenetic products was guided by their presence, abundance and potential variability, as well as by outcrop conditions. Except for the Obernberg rockslide (see Table 1), where poor outcrop and scarce lithification allowed for excavation of three samples only , between 12 to 42 samples were taken per rockslide. Polished rock slabs and a total of 82 thin sections provided petrographic data on diagenesis. Dark-field microscopy was done on an Olympus SZX10 binocular. Electron microscopic inspection of unsputtered samples of abrasive rock dust was done with a Digital Scanning Microscope JEOL JSM-5130LV in low-vacuum mode, at 25 kV acceleration voltage, a current of 5 μA, with a backscattered electron detector.

For measurement of stable isotopes of oxygen and carbon of diagenetic products and host rocks, samples were excavated from polished slabs with a microdrill. The mass of individual samples weighed for measurement ranged from 5 to 25 mg. Samples were weighed to a precision of ±0.25 μm on a Mettler Toledo UMT2 microbalance, and transferred into round-bottomed borosilicate exetainers. The exetainers then were sealed with butyl rubber septa, and placed into a CTC Combi-Pal autosampler. Measurements were made on a Finnigan Delta^{plus}XL mass spectrometer connected to a ThermoFinnigan GasBench II. The internal precision (1 sigma) of measurement is typically between 0.03–0.06 for raw $\delta^{13}C$, and 0.04–0.08‰ for raw $\delta^{18}O$; the external precision, calculated over 12 standards per run, typically is 0.05–0.06‰ for $\delta^{13}C$ and 0.06–0.08‰ for $\delta^{18}O$. The in-house standard material 'Laas marble' has been calibrated to reference materials NBS-18, NBS-19, CO-1 and CO-8 (see Spötl and Vennemann, 2003, for further details). To determine the mineralogy of micritic cements, to differentiate 'impure' mixtures of newly precipitated micrite plus clastic minerals from the rockslide mass, and to determine the polymorphy of fibrous calcium carbonate cements, X-ray powder diffractometry was applied to some samples. XRD analyses were performed on an AXS-Bruker D-8 diffractometer (Cu-target, E-dispersive counter, parallel beam optics) at 40 kV and 40 mA.

During the geological exploration for the Brenner base-tunnel (Brandner et al., 2008), the rockslide mass of Pfitsch Valley (Fig. 1, Table 1) was drilled. Drilling Vi-B-09/04 was performed as a rotary core drill, with a Wirth B1 equipment. The drilling terminated at 409 m depth; from zero to 83 m depth, drilling proceeded within the lithified rockslide mass. Two samples of lithified rockslide material were taken from the drill core at 23.5 m below ground surface. The rockslide mass, however, is lithified down to its base at −83 m. From −83 m to a final depth at −409 m, the rockslide is underlain by *in-situ* bedrock calcphyllites with intercalated layers of greenschist. The other samples from the Pfitsch Valley rockslide were taken from surface outcrops.

3. Rockslide lithification

The most widespread style of partial lithification of rockslide deposits is represented by lenses of breccias adherent to the overhanging flanks and undersides of boulders ('under-boulder breccias', Table 2; Fig. 2A and B). The under-boulder breccias may contain relict patches of fine-grained cataclastic matrix produced by dynamic disintegration during the rockslide event. Most commonly, however, the pore space between lithoclasts is partly or entirely filled by diverse types of cement. From the surface of a boulder outward/downward, cementation tapers out within a few centimeters to a few decimeters. The interstitital cements include crusts of micritic to micropeloidal cement, calcitic orthospar cements or, as in Fern Pass rockslide, fibrous aragonite (Table 3). Along the underside of boulders, towards megapores up to a few centimeters in width, isopachous fringes of cement, soda-straw stalactites up to a few centimeters in length, and flowstone-like 'curtains' of cement may be present (Fig. 2C and D and E). Cement fringes include micritic cement, stout-prismatic calcite cements, and layers and pendant fabrics of fibrous cement (Fig. 2C and D and E). The under-boulder cements may be topped by digitate to arborescent crusts of clotted to faintly laminated micrite (Fig. 2F); this is the case where boulder undersides became exposed to daylight by natural hillslope erosion and/or along man-made outcrops (roadcuts, gravel pits). Identical micritic crusts have been observed also on episodically wet, daylit lateral flanks of boulders. Alternatively, the under-boulder cements may be overlain by a layer of micrite arranged in alveolar septal structures (Fig. 2E). To date, under-boulder breccias and cements were observed only with boulders that project from the surface of the rockslide deposit.

The rockslide deposit of Tamins (Fig. 1, Table 1) is topped over large parts of its extent by a layer of breccia up to about 1.5 m in thickness. The breccia layer is concordant with the irregular, subhorizontal to steeply dipping surface of the rockslide deposit, and is present irrespective of boulders (Figs. 2G and 3). After its descent, the Tamins rockslide had dammed up a lake (Lake Bonaduz; von Poschinger, 2005). Subsequently, when the younger Flims rockslide (cf. Table 1) descended into Lake Bonaduz, both water and lacustrine deposits were pushed out in a catastrophic flood that overrode the Tamins rockslide mass (Fig. 3A; Pavoni, 1968; von Poschinger et al., 2006). The contact between the breccia layer on top of the Tamins rockslide and the overlying unlithified flood deposits is sharp. In a formerly open man-made outcrop, the top surface of the breccia layer, in contact to the flood sediments, was seen to be striated and grooved (von Poschinger and Kippel, 2009, their Fig. 12). At several locations, man-made outcrops show that the breccia layer is also overlain by other unlithified deposits formed long after the mass-wasting event; such deposits include stratified talus slopes and hillslope colluvium derived from subaerial erosion of the rockslide mass (Fig. 3B). Internally, the breccia may consist of rockslide lithoclasts embedded in a matrix of lithified cataclastic gouge (Figs. 2H and 4A). Alternatively, the lithified matrix is confined to patches only whereas most of the interstitital pore space is filled by micritic cement and/or calcite spar cement. There is a continuum from (a) breccia fabrics with cataclastic gouge lithified *in-situ* (rockslide breccia *s. str.*) to (b) fabrics partly overprinted by eluviation–dissolution of cataclastic matrix, followed by precipitation of cement, to (c) fabrics in which the cataclastic matrix has been removed by eluviation–dissolution, and the resulting pore space became filled by cement (Fig. 4B). Along the underside of larger boulders, the breccia is mainly lithified by calcite spar cement.

In Pfitsch Valley (Fig. 1, Table 1), a rockslide deposit is lithified from its present top down to its base 83 m below surface, as revealed by a drill core (Fig. 5). This rockslide is composed of calcphyllites mainly of calcite, quartz, chlorite, muscovite and accessory pyrite ('Bündner Schiefer' of Alpine geological literature) (Höck and Hoschek, 1980). The Bündner Schiefer originally represented mixed siliciclastic–carbonate turbidite deposits (Frisch et al., 1987). In the field and in cut slabs, the rockslide deposit is characterized by a lithified cataclastic gouge of brown tint (Fig. 4C). The cataclastic gouge was mainly produced by shearing and cataclasis of the calcitic domains of the calcphyllite; the quartzose domains, by contrast, disintegrated by fracture into discrete grains (Fig. 4D). Throughout the observed portions of the rockslide mass, the fabric is characterized by abundant micropores to megapores up to a few millimeters in width. Significant dissolution of calcite is recorded by selective removal of calcite domains from, both, clasts of calcphyllite and

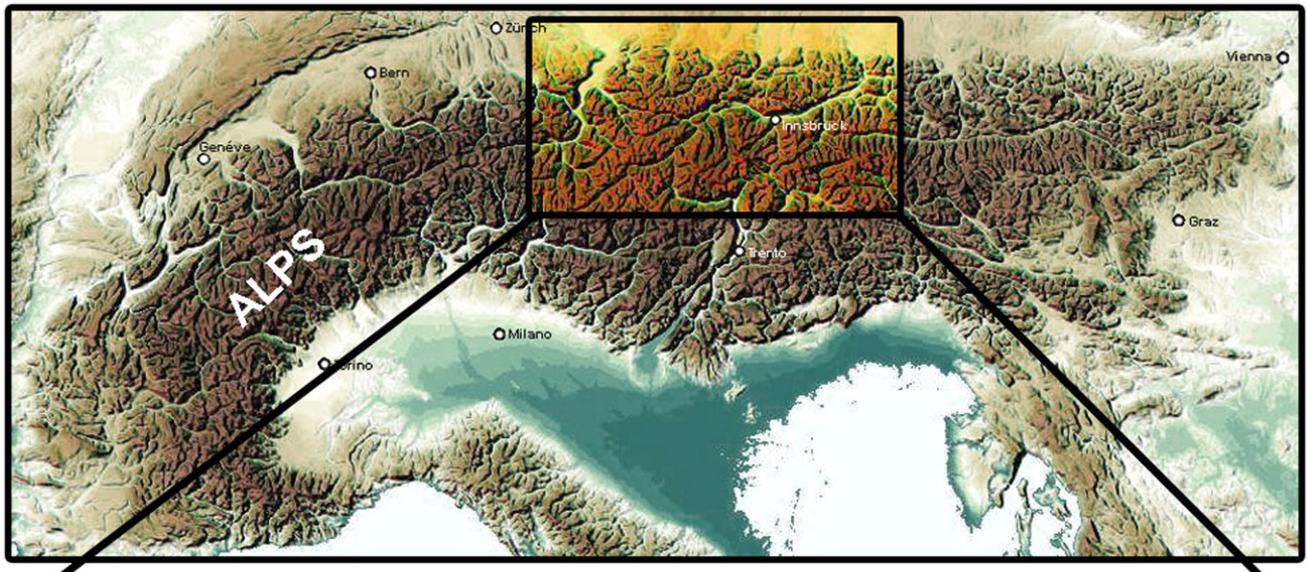

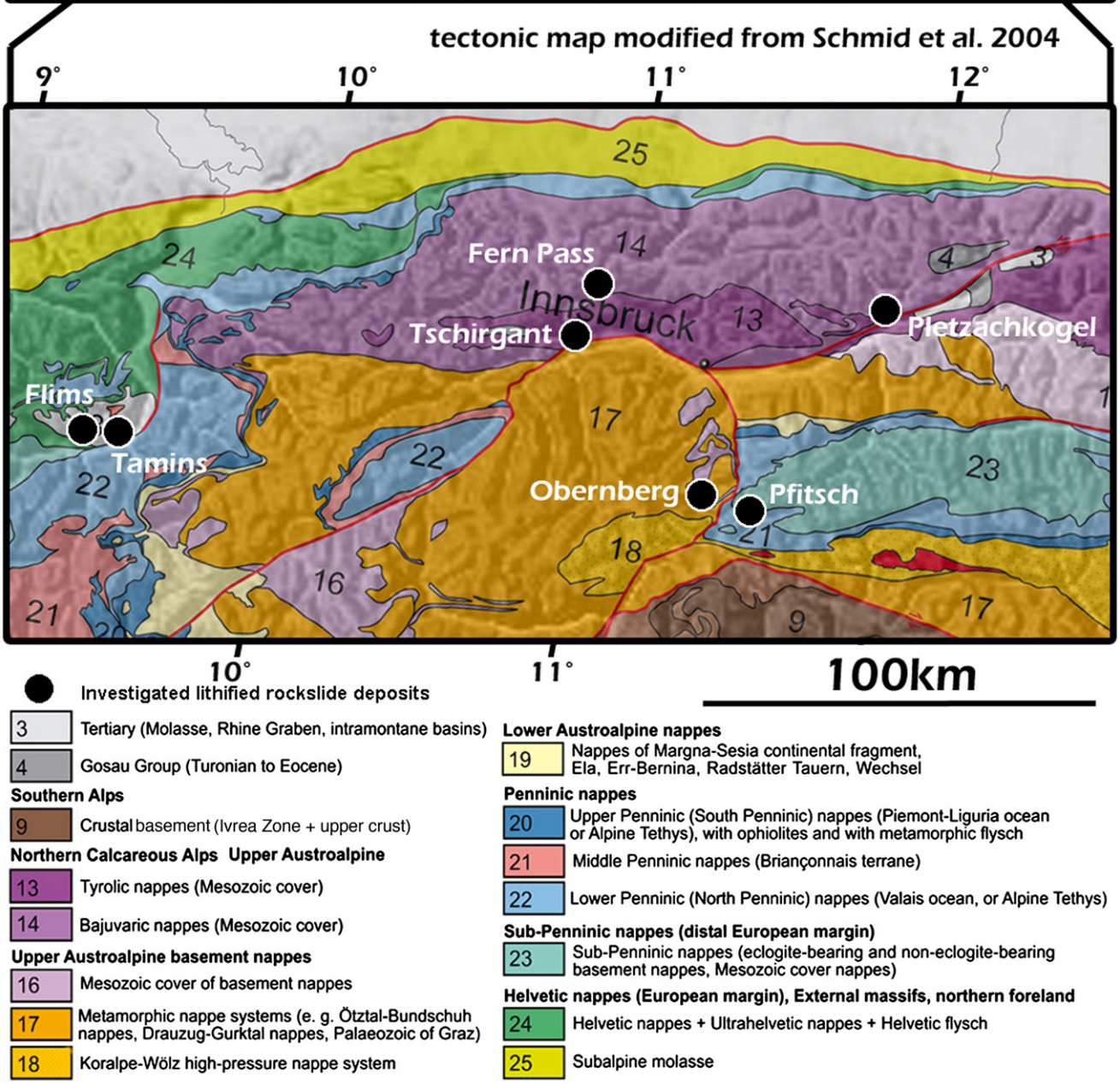

Investigated lithified rockslide deposits

3 Tertiary (Molasse, Rhine Graben, intramontane basins)

4 Gosau Group (Turonian to Eocene)

Southern Alps

9 Crustal basement (Ivrea Zone + upper crust)

Northern Calcareous Alps Upper Austroalpine

13 Tyrolic nappes (Mesozoic cover)

14 Bajuvaric nappes (Mesozoic cover)

Upper Austroalpine basement nappes

16 Mesozoic cover of basement nappes

17 Metamorphic nappe systems (e. g. Ötztal-Bundschuh nappes, Drauzug-Gurktal nappes, Palaeozoic of Graz)

18 Koralpe-Wölz high-pressure nappe system

Lower Austroalpine nappes

19 Nappes of Margna-Sesia continental fragment, Ela, Err-Bernina, Radstätter Tauern, Wechsel

Penninic nappes

20 Upper Penninic (South Penninic) nappes (Piemont-Liguria ocean or Alpine Tethys), with ophiolites and with metamorphic flysch

21 Middle Penninic nappes (Briançonnais terrane)

22 Lower Penninic (North Penninic) nappes (Valais ocean, or Alpine Tethys)

Sub-Penninic nappes (distal European margin)

23 Sub-Penninic nappes (eclogite-bearing and non-eclogite-bearing basement nappes, Mesozoic cover nappes)

Helvetic nappes (European margin), External massifs, northern foreland

24 Helvetic nappes + Ultrahelvetic nappes + Helvetic flysch

25 Subalpine molasse

Table 1
Investigated rockslide deposits, arranged by position on major tectonic units of the Alps (see Fig. 1). See text for definition of rockslide types and Tables 2 and 3 for further characterization of diagenetic phenomena. For an overview of Alpine orogenesis and tectonostratigraphic units see Schmid et al. (2004).

Rockslide location Type of rockslide Altitude range of surface exposure of rockslide deposits	Tectonostratigraphic unit Chronostratigraphic range	Age and lithologies of rockslide deposit Metamorphic grade	Diagenetic phenomena	Age of rockslide event(s), dating method, references
Fern Pass Rock avalanche 1330–800 m asl	Northern Calcareous Alps; Upper Austroalpine unit Lower Triassic to Jurassic (locally Cretaceous–Tertiary)	Upper Triassic dolostones, limestones, marls Non-metamorphic	Under-boulder breccias	4200–4100 a $^{234}U/^{230}Th$ of 'under-boulder cement' in rockslide deposit, ^{36}Cl dating of exposed scarp; both numerical ages overlap (Ostermann et al., 2007; Prager et al., 2009)
Pletzachkogel Rock avalanche 900–520 m asl		Lower Jurassic limestones Non-metamorphic	Under-boulder breccias	Three rockslide events, at: 15,500 ± 500 ^{14}C cal BP; 3910 ± 479 ^{14}C cal BP; 1735 ± 135 ^{14}C cal BP (Patzelt, 2004a,b, in: Prager et al., 2008)
Tschirgant Rock avalanche 850–680 m asl		Middle to Upper Triassic dolostones, limestones, cellular dolomites Non-metamorphic	Under-boulder breccias, flowstones	First date: about 2900 ^{14}C a BP (Patzelt and Poscher, 1993); later age-dating suggested two rockslide events, at: 3753±191 ^{14}C cal a BP 3151± 359 ^{14}C cal a BP (Patzelt, 2004a, in: Prager et al., 2008) $^{234}U/^{230}Th$ ages from 'under-boulder' soda-straw stalactites from two different locations: 3650 ± 350 a; 2800 ± 100 a; two rockslide events may also be suggested by the U/Th ages (Ostermann and Sanders, 2009)
Obernberg Rock avalanche 1780–1360 m asl	Central-Alpine Mesozoic; Upper Austroalpine unit Lower Triassic to Lower Jurassic	Upper Triassic calcitic marbles Medium-grade metamorphic	Under-boulder breccias (poorly developed)	Post-Glacial: no numerical age established
Pfitsch Valley Rock avalanche 1560–1260 m asl	Penninic unit Early Jurassic to Paleogene	Calcphyllites mainly of calcite, chlorite, quartz and muscovite Medium-grade metamorphic	Widespread to ?wholesale lithification of rockslide mass	Post-Glacial: No numerical age established
Flims (largest rockslide in the Alps) Rockslide 1500–600 m asl	Helvetic unit Lower Triassic to Paleogene	Jurassic metalimestones Low-grade metamorphic	(a) Cementation of talus slopes and fluvial conglomerates, (b) emergence of limestone-precipitating springs from rockslide	9455 ± 25 ^{14}C cal a BP (Deplazes et al., 2007)
Tamins Rock avalanche 860–600 m asl	Helvetic unit Lower Triassic to Paleogene	Jurassic metalimestones Low-grade metamorphic	Surficial layer of breccia, under-boulder breccias	No age established; older than Flims rockslide (see above) (von Poschinger et al., 2006)

from the gouge matrix. Open dissolution macro- to megapores with deeply-embayed and pitted solution relicts of calcite are widespread. Visual comparison with porosity estimators in Flügel (2004) indicates between about 10–30% porosity, down to the base of the rockslide. The dissolution pores invariably are devoid of sparitic cement. The lithification of the rockslide deposit seems to be entirely imparted by lithification of the cataclastic gouge. The rockslide mass is cut by a subvertical fault. Fault displacement is recorded by systematic tilting of rockslide clasts adjacent to the fault plane. The cause for faulting of the Pfitsch Valley rockslide mass is unclear. The fault may result from neotectonism and/or from gravity-induced deformation. Along an open joint associated with the fault, a veneer of prismatic calcite cement formed that was sampled for U/Th age-dating (Fig. 4E).

The distal-most preserved part of the rockslide mass of Tamins is represented by a few tuma hills (Fig. 3A) composed of micaceous calcphyllites with accessory pyrite. Tuma hills are a common feature of rockslides. Tumas are cone-shaped to elongate, steep-flanked hills composed of rockslide material, and typically are detached from the majority of the rockslide mass. Tuma hills commonly are a few tens of meters in height (cf. Abele, 1974). The calcphyllites of the distal-most tumas of the Tamins rockslide are derived from a tectonic sliver of Variscan metamorphic rocks cropping out near the toe of the detachment scar. Similar to Pfitsch Valley, these tumas are lithified, and show a brown tint both in the field and in cut slabs. In a thin section, the fabric of the lithified tumas is similar to the Pfitsch rockslide in that they show a highly porous fabric, thin crusts of micritic cement around clasts, and solution pores after calcite (Fig. 4F).

Fig. 1. Location of rockslide deposits investigated for lithification. The colour and letter codes of structural units are taken from Schmid et al. (2004).

Table 2
Field phenomena of diagenesis observed in carbonate-lithic rockslide deposits.

Type	Characterization	Interpretation	Remarks
Under-boulder breccias	Breccias composed of clasts of rockslide material. Breccias adhere to flanks and undersides of boulders that project from the rockslide deposit. Cementation tapers out outward and downward.	Meteoric dissolution of (a) abrasive carbonate (mini-) micrite, and (b) of the boulders themselves, followed by re-precipitation of calcium carbonate on boulder flanks and undersides	Most widespread phenomenon of lithification. Confined to topmost few meters of rockslide masses.
Isopachous crusts of carbonate cement, soda-straw stalactites, and flowstone-like 'curtains' of cement on undersides of boulders	Crusts, small stalactites, and small curtains of micritic to sparitic calcite on the undersides of boulders that project from the rockslide deposit.	Meteoric dissolution of abrasive carbonate (mini-) micrite and of the boulder, followed by re-precipitation of calcium carbonate on the underside of the boulder	Typical for Tschirgant rockslide
Surface-concordant layer of breccia composed of rockslide material	Layer up to 1.5 m thick of breccia composed of rockslide material. Breccia layer is (a) concordant with surface of rockslide, (b) locally overlain by unlithified deposits (e. g. talus slopes) derived from later erosion of the rockslide mass	Lithification by dissolution of fine-grained abrasive carbonate micrite, followed by re-precipitation of calcium carbonate. Lithification started closely after the rockslide event.	Observed only at Tamins rockslide.
Extensive (wholesale?) lithification	Large parts of rockslide mass lithified, but abundant micro- to megaporosity. Supports vertical to overhanging cliffs.	Lithification driven by (a) carbonate dissolution caused by oxidation of pyrite, followed by (b) re-precipitation of part of the dissolved calcium carbonate.	Observed for (a) Pfitsch Valley, (b) Tamins rockslide
Fracture cement	Cement fringes formed along the walls of fractures within the rockslide mass	Precipitation of carbonate cement along open joints in lithified rockslide mass, in essentially phreatic diagenetic environment	Observed only in Pfitsch Valley rockslide

4. Lithification of post-rockslide ('secondary') deposits

Most rockslide masses undergo substantial geomorphic changes, for instance, by river incision and disintegration by sliding, slumping, and toppling. Erosion of a rockslide mass may result in 'secondary' deposits such as talus slopes or fluvial successions that onlap the erosional surface. Along deep fluvial gorges incised into the Flims rockslide, onlapping talus slopes and fluvial gravels are

Table 3
Microscopic features of diagenesis in rockslide deposits.

Type	Characterization	Interpretation	Remarks
Lithified rockslide matrix	Micritic to siltitic matrix with grains of rockslide host lithologies. May be grain- or matrix-supported	Lithification by micrometer-scale dissolution and re-precipitation of abrasive matrix generated during rockslide movement	Uncommon. Resulting fabric designated as 'rockslide breccia'. Figs. 2G and H, 4A and C and D
Micritic cement	Isopachous to mammillary, non-laminated or 'wrinkly'-laminated crusts of lime mudstone	Cement formed in meteoric-vadose environment	Common. Figs. 2E and 4F
Micropeloidal grainstones to packstones	Mammillary crusts around rockslide clasts, and faintly geopetally-oriented infills in interstitial pore space of under-boulder breccias	Microbial cement (mammillary crusts) and calcified microbial aggregates (geopetally-oriented infills) in in interstitial pore space	Uncommon. See Ostermann et al. (2007)
Fringes of botyroidal aragonite cement	Isopachous to boytroidal fringes of fibrous aragonite cements	Aragonite cements formed in 'under-boulder setting' by evaporation of meteoric-vadose waters with high Mg/Ca ratio (Ostermann et al., 2007)	To date observed only in the Fern Pass rockslide composed of dolostone clasts. See Ostermann et al. (2007)
Calcitic spar cements	(1) Isopachous fringes of calcite spar (2) Fringes or crusts of prismatic calcite spar	Precipitation of calcite in an effectively meteoric–phreatic environment, from pore waters with a low Mg/Ca ratio	(1) Common. Fig. 4B (2) Observed in Pfitsch Valley rockslide mass on joint plane. Fig. 4E
Soda-straw stalactites, flowstone curtains	(1) Soda-straw stalactites up to a few cm in length of prismatic calcite spar, present on undersides of larger boulders (2) Flowstone curtains composed on prismatic calcite spar, present on undersides of larger boulders	Precipitation of calcite in clast-supported 'under-boulder microcaves', in an effectively meteoric–phreatic environment, from waters with a low Mg/Ca ratio	Uncommon, to date observed mainly in Tschirgant rockslide. Fig. 2C and D
Solution porosity	(a) Micro- to megapores mainly within matrix. (b) Micro- to megapores selective after the calcite component in pyritiferous rocks, with deeply-embayed and pitted dissolution relicts of calcite.	(a) Dissolution pores after fine-grained matrix produced by dynamic cataclasis of carbonate rocks (limestones, dolostones). (b) Dissolution pores after calcite produced by oxidation of pyrite.	(a) Minor solution porosity is common. Fig. 4A and B (b) To date observed only in the Pfitsch Valley rockslide. Expectably common in rockslide deposits composed of pyritiferous rocks rich in carbonate minerals. Fig. 4C

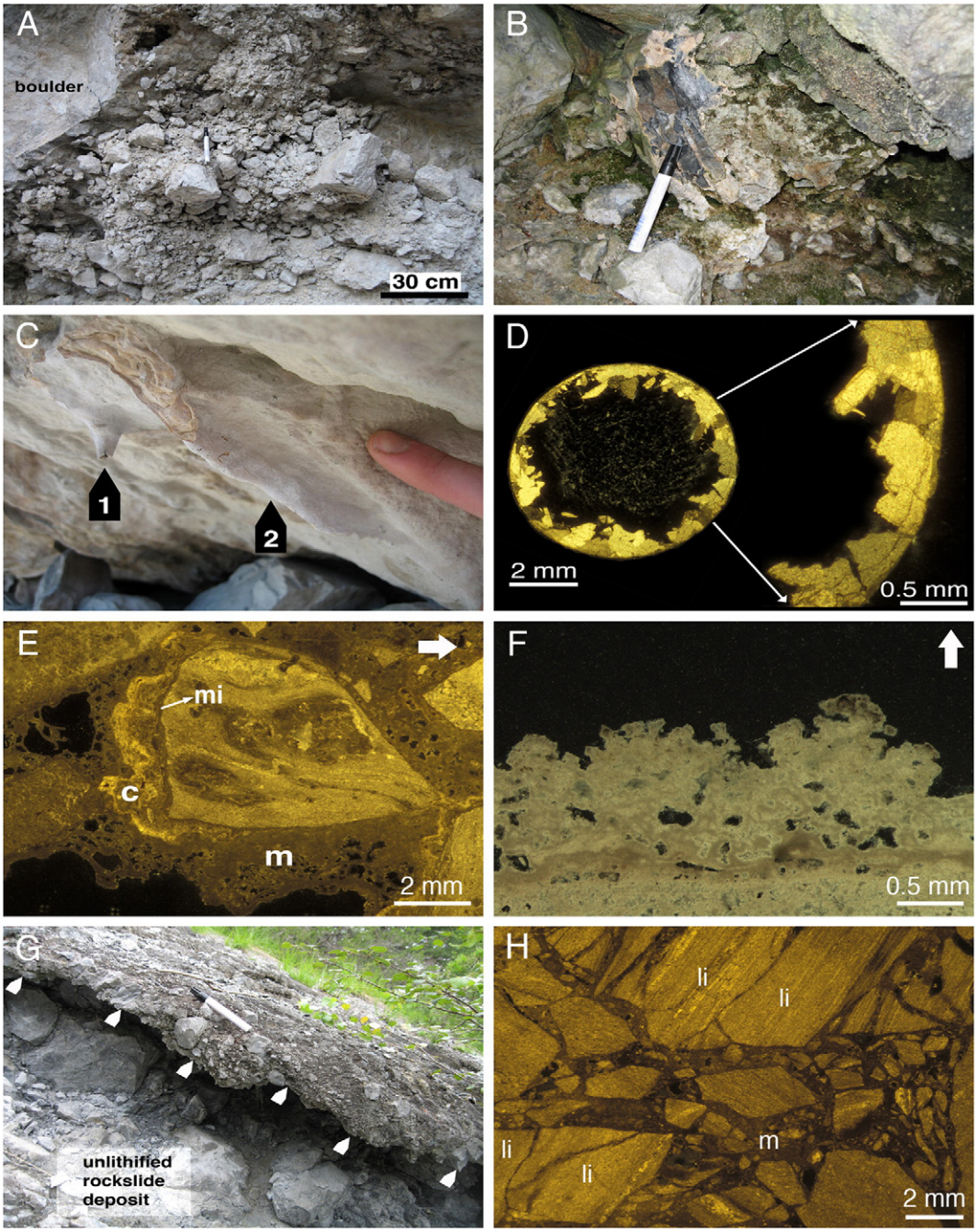

Fig. 2. A. Breccia composed of rockslide lithoclasts. The breccia formed along and is confined to the lower flank and underside of a large boulder (under-boulder breccia, see text). Tschirgant rockslide. B. Under-boulder breccia lithified by crusts of carbonate cement, overlain by a greenish to grey carbonate crust. Tamins rockslide. Pen is 14 cm in length. C. Small soda-straw stalactite (1) and incipient flowstone curtain (2) on the underside of a boulder. Tschirgant rockslide. D. Thin section of cross-section through a soda-straw stalactite from the underside of a boulder. The stalactite consists of equant to prismatic calcite crystals that grew from the outer surface of the stalactite towards its center. Crossed nicols. Tschirgant rockslide. E. Thin-section image of under-boulder breccia shown in B: Lithoclasts are cemented by a thin fringe of micritic cement (mi), pendant fabrics of flowstone cement (c), overlain by micrite (m) with an alveolar fabric. Crossed nicols. Arrow points to top. F. Detail of micrite layer with digitate to stout-arborescent fabric. This micrite layer overlies a crust of flowstone cement on the underside of a boulder. Darkfield, crossed nicols. Arrow points in gravity direction. Tschirgant rockslide. G. Layer of breccia composed of rockslide material. The breccia layer dips very steeply, concordant with the local slope of the rockslide mass. The breccia marked by white arrows is underlain by unlithified, backweathering rockslide material of identical clast spectrum and fabric. Tamins rockslide. Pen is 14 cm in length. H. Photomicrograph of breccia layer on top of rockslide mass, Tamins. Note that many of the lithoclasts (a few labeled li) show fitted clast boundaries. The matrix (m) is a lithified cataclastic gouge down to micrite size. Grain size grades from lithoclasts to micrite. Crossed nicols.

lithified by well-developed meteoric-vadose cements (Fig. 6A and B). Both in talus slopes and in fluvial gravels, cementation is confined to the proximity of the rockslide mass. In addition, limestone-precipitating springs locally emerge out of the Flims rockslide deposit.

5. Stable isotope values of oxygen and carbon

The isotope shift of oxygen and carbon from host rocks to cements are classified into three groups (Fig. 7): (1) cements that record a shift in carbon isotopic ratios, but little shift in oxygen

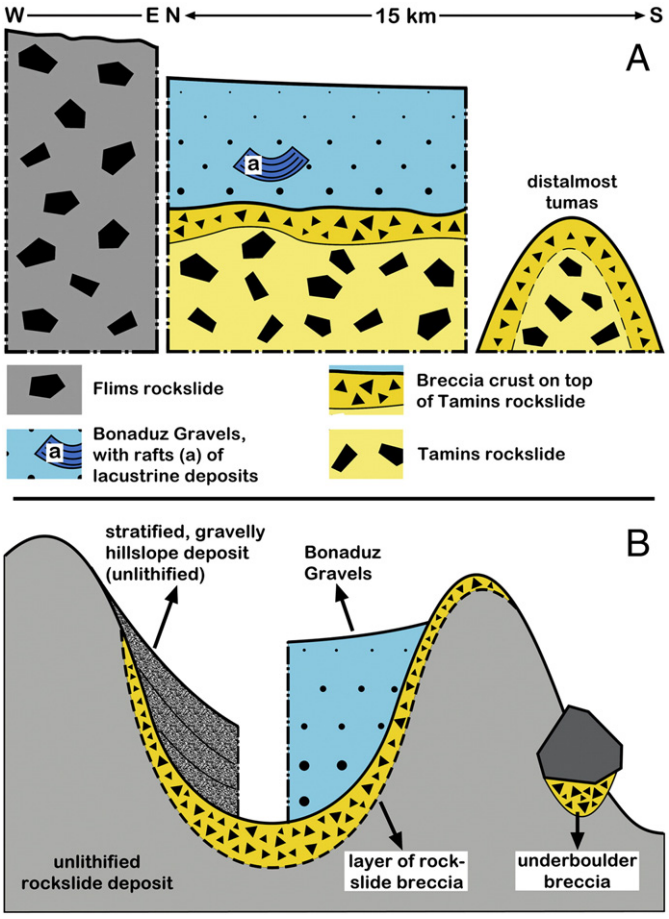

Fig. 3. Schematic succession in the Tamins–Flims area (cf. Fig. 1). A. Out to its distal-most tuma hills, the Tamins rockslide is topped over a large part of its extent by a layer of breccia. The breccia layer is in sharp contact with the overlying unlithified Bonaduz Gravels; these gravels accumulated during a catastrophic flood when the younger Flims rockslide (see Table 1) pushed out a lake dammed up by the Tamins rockslide. B. In the Tamins rockslide mass, the breccia layer on top is overlain by stratified gravelly hillslope deposits or by hillslope colluvium, or by the Bonaduz Gravels. Where the breccia layer is absent, 'under-boulder breccias' are present.

isotope values, (2) cements that record a co-variant shift towards more negative values of both carbon and oxygen, and (3) aragonite cement with a high-positive carbon isotope value relative to the host rock. The implications of the stable isotopes values are interpreted farther below.

6. Interpretation

6.1. Patterns of lithification

The meteoric lithification of rockslides proceeds in a 'donor–acceptor' mode whereby cement precipitation is nourished by calcium carbonate dissolution at another site typically nearby (Bathurst, 1975). During the descent of a rockslide, within the moving mass, the rocks are subject to intense fracturation in the process of dynamic disintegration (McSaveney and Davies, 2002; Pollet and Schneider, 2004; Imre et al., in press). In addition, rockslide descent is associated with huge airborne clouds of rock dust; in settling, the dust forms a 'snow-like' drape up to more than 10 cm in thickness (Fig. 6C) (Heim, 1932). Even rock*falls* can produce square-kilometer-sized dust clouds. SEM inspection of dolomite rock powder settled from the dust cloud of a 60,000 m^3 rockfall (in the Dolomite mountains, Northern Italy, on October 12th, 2007) showed that the dust consists of minimicritic (less than 1 μm in size; Folk, 1974) to fine sand-sized particles (Fig. 6D). Fine-grained particles produced by fracture are supersoluble (cf. Anderson et al., 2000; Skidmore et al., 2004). Thus, normal rainfall with a pH of about 5.6 to 5.4 (Berner and Berner, 1996) onto pristine rockfall-generated dust should result in a very shallow-meteoric-vadose water highly charged in dissolved carbonate. Most lithification in shallow levels of rockslide deposits thus may start immediately after the event, when highly reactive rock powder is still abundant (cf. Prager et al., 2009).

The common presence of under-boulder breccias points to a causal relation between boulders and breccias. In coarse-grained fabrics such those of rockslides, interstitial water percolates downward at a rate of decimeters to meters per day (Hölting and Coldewey, 2005). No data are available on evaporation–precipitation budgets in rockslide areas. By analogy to the well-documented effect of soil mulches (cf. Yamanaka et al., 2004), however, we suggest that the main effects of boulders in favouring re-precipitation of dissolved carbonate are: (a) collection of precipitation and focusing of runoff mainly along the boulder flanks, and (b) retention of water in the under-boulder domain, by retarding evaporation, and by slow seepage of water out from the boulder (Fig. 8). During rain or snow melt, water plus dissolved carbonate rapidly percolates downward into the rockslide. This downward transport in most cases obviously does not lead to carbonate re-precipitation deeper within the rockslide mass. Conversely, in the under-boulder setting, subsequent to rain or snow melt, the boulder will slowly seep out carbonate-saturated water along joints and bedding planes over a prolonged interval of time while evaporation aids in carbonate re-precipitation. Carbonate dissolved from, both, the rockslide matrix and the boulders thus has opportunity to re-precipitate as a cement, and is sheltered from dissolution during a subsequent infiltration phase. The digitate to arborescent crusts of porous micrite that locally overlie the under-boulder cements may represent lichen stromatolites (Klappa, 1979). Lichens can start to grow and calcify when the under-boulder flank becomes exposed to daylight. This interpretation is supported by the observation that such crusts seem to be absent along boulder undersides exposed recently by human activity, such as in gravel pits. The micritic alveolar septal structure of micrite is more difficult to interpret. Where clearly associated with rhizocretions or rhizoliths (Klappa, 1980), alveolar septal structure can be interpreted as a result of fungal and/or microbially-induced precipitation of micrite in the halo around a root (Alonso-Zarza et al., 2008). Because we did not observe rhizocretions in our samples, we prefer to interpret these alveolar structures as a result of fungal and/or lichen-induced calcification (cf. Wright, 1989; Burford et al., 2003).

For the breccia layer of Tamins, different effects than sheltering by boulders must be invoked. The concordance of the breccia layer with the surface of the rockslide deposit suggests two explanations. (1) The breccia formed readily after rocksliding, upon dissolution and re-precipitation of chemically reactive rock powder. (2) A lithification process similar to caliche may have been active. In caliche profiles of (semi-)humid climates, carbonate dissolved in the upper soil level becomes re-precipitated deeper in the profile. In none of our samples of the breccia layer, however, did we observe structures indicative of caliche, such as faintly laminated fenestral micritic crusts, micritic nodules and rhizolithic levels (cf. Wright, 1989, 1994). There is also no evidence that processes such as soil-related micritization and sparmicritization (Kahle, 1977) caused breccia formation. As mentioned above, the surface of the breccia layer is sharp and, locally, grooved and striated in contact to overlying flood sediments. The numerical age of the Tamins rockslide is not established so far, but there is general agreement that it took place shortly before the younger Flims rockslide (dated at 9455 ± 25 cal a BP; Deplazes et al.,

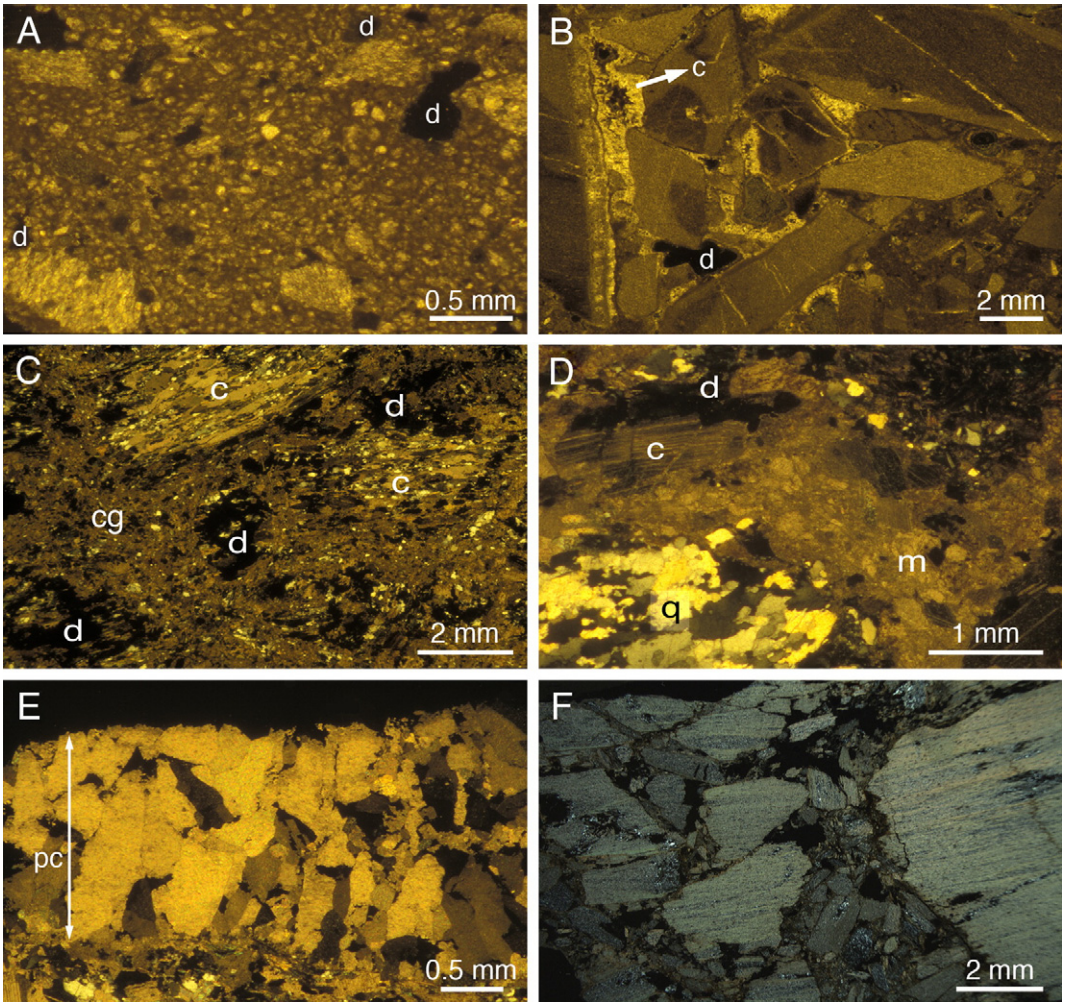

Fig. 4. A. Photomicrograph of lithified matrix of breccia layer on top of Tamins rockslide mass, Tamins. The matrix consists of a cataclastic gouge down to micrite size, and is riddled by dissolution micro- to macropores (a few labeled d). Crossed nicols. Width 3 mm. B. Photomicrograph of breccia layer on top Tamins rockslide. In this sample, the interstitial cataclastic matrix has locally been removed by eluviation and/or dissolution; the resulting pore space became largely filled by a fringe of scalenohedral calcite cement (c). Also note dissolution pore (d). Crossed nicols. C. Photomicrograph of rockslide breccia composed of clasts of quartz-bearing calcphyllite. Clasts of more-or-less intact calcphyllite (c) float in a porous matrix of lithified cataclastic gouge (cg). The matrix consists of a gouge of carbonate minerals (mainly calcite), with floating grains of quartz. Note dissolution pores (d) after clasts of calcphyllite. Crossed nicols. Pfitsch Valley rockslide. D. Photomicrograph of rockslide breccia, showing intact lense of polycrystalline quartz (q) embedded in lithified matrix (m) of cataclastic gouge derived from disintegration of calcite. Note also fracture and twinning of partly preserved calcite crystal (c) adjacent to a dissolution pore (d). Crossed nicols. Pfitsch Valley rockslide. E. Photomicrograph of a layer of prismatic calcite (pc, indicated by white arrow) that formed at the surface of a normal fault cutting a lithified rockslide deposit composed of clasts of calcphyllite. Crossed nicols. Pfitsch Valley rockslide. F. Photomicrograph of rockslide breccia composed of clasts of mica schist with accessory calcite. The highly porous breccia is lithified by a very thin fringe of micrite derived by dissolution of the calcite. Crossed nicols. Tamins rockslide.

2007; von Poschinger et al., 2006). The total evidence from field to thin section thus seems consistent with a relatively rapid formation of the breccia crust, probably by dissolution/re-precipitation of rock powder. An early diagenetic origin is also supported by the identity in clast spectrum and interstitial matrix of steep-dipping portions of the breccia crust with the directly underlying, unlithified rockslide mass. In addition the locally overlying, unlithified, stratified hillslope deposits shows a different inventory of textures and organization into strata as typical for talus slopes (cf. Sanders et al., 2009a). The unlithified talus slopes that accumulated above the steep-dipping portions of the rockslide mass today are covered by forest; yet, lithification is sharply confined to the underlying breccia crust. This underscores that breccia lithification started early, perhaps immediately after the rockslide event, but decelerated later on. This is consistent with the hypothesis that rockslide lithification is mainly driven by highly soluble rock particles that become exhausted with time. We concede that the ultimate reasons are not yet fully clear why in one case, only under-boulder breccias and in another case, a breccia layer should form by the same process of dissolution/re-precipitation of fine-grained cataclastic material. We suspect, however, that the difference is mainly related to different lithologies of and different microclimatic conditions affecting rockslide deposits. Because infiltrating meteoric water probably attains $CaCO_3$ saturation within decimeters to meters from the surface, when percolated deeper into a rockslide mass, little or no chemical change occurs. Only where the 'deep' meteoric groundwater is subject to CO_2-degassing and evaporation, such as upon its re-emergence out from the rockslide mass along the flanks of incised valleys, re-precipitation of calcium carbonate will take place. This is supported by: (a) the cementation of 'secondary' deposits (talus slopes, fluvial gravels) along and near their onlap onto carbonate-lithic rockslide masses, and (b) the emergence of limestone-precipitating springs from rockslide deposits.

As described, the lithified rockslide deposits of Pfitsch Valley composed of calcphyllites show a highly porous fabric rich in solution relicts of carbonate minerals, and lack fringes of cement.

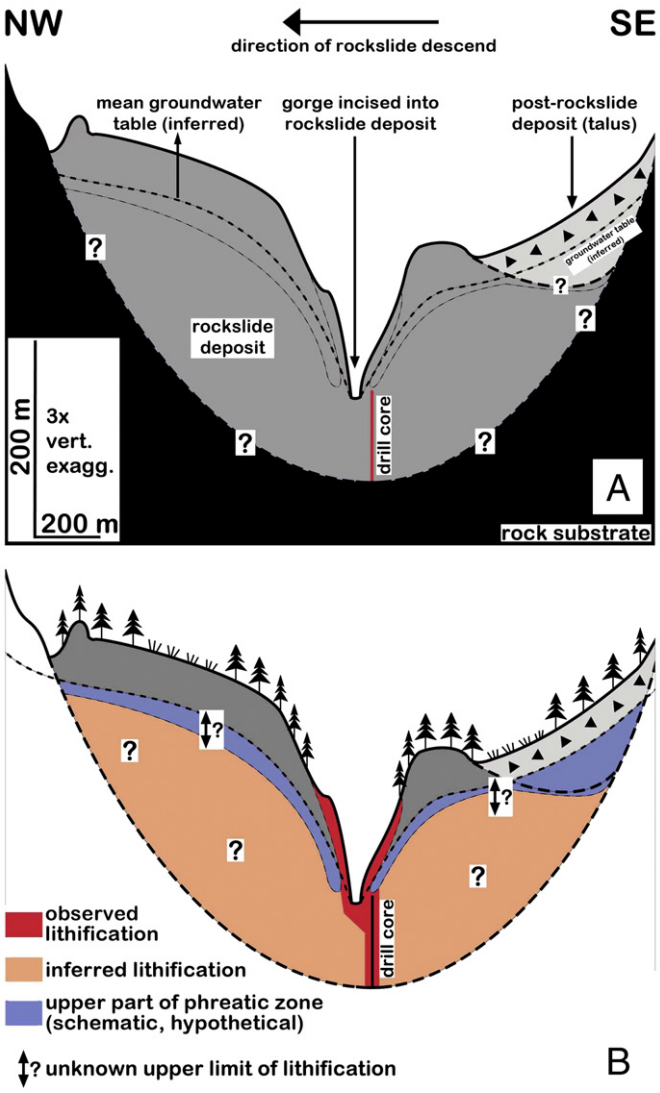

Fig. 5. Schematic cross-section of Pfitsch Valley rockslide (A) (cf. Fig. 1, Table 1), and its lithified and potentially lithified portions (B). This rockslide is the most extensively lithified known to the authors. See text for further description and discussion.

In these lithologies, in addition to carbonate dissolution according to Eq. (1), pyrite oxidation may drive further dissolution, according to:

$$4FeS_2 + 15O_2 + 8H_2O + 16CaCO_3 \Rightarrow 2Fe_2O_3 + 16Ca^{2+} + 8SO_4^{2-} + 16HCO_3^- \quad (1)$$

(Berner and Berner, 1996, p. 164)

The Fe_2O_3, practically insoluble in oxygen-bearing groundwater, gives the characteristic ocre to brown colour to the lithified rockslide deposits. Of the other reaction products, calcium sulfate seems to be too soluble to precipitate within the rockslide mass. Finally, part of the calcium carbonate dissolved upon, both, 'normal' meteoric dissolution and pyrite oxidation probably re-precipitates within the rockslide deposit, to impart lithification.

6.2. Stable isotope values

The illustrated patterns of isotope shift from host rocks to cements (Fig. 7) may reflect different processes of isotope fractionation. In the highly variable diagenetic environment in the shallowmost portions of rockslides, stable isotopes probably are subject to kinetic fractionations. High solubility of fine-grained particles results in kinetic carbon fractionation during early dissolution, but is also dependent on the $CaCO_3$/water ratio; kinetic fractionation will dominate the dissolved inorganic carbon isotope signal in environments of short (hours to days) contact between carbonate-dominated sediment and water (Skidmore et al., 2004; Jiménez-López et al., 2001). Both, short-term sediment/water contacts and carbonate-dominated sediment, are met in the near-surface environment of carbonate-lithic rockslides.

6.2.1. Shift pattern 1

This pattern of isotope shift may indicate that these cements precipitated mainly due to CO_2-degassing from water (cf. Lohmann, 1988). This seems consistent with the fact that these cements include soda-straw stalactites and incipient flowstone curtains.

6.2.2. Shift pattern 2

This pattern may record an influence of both CO_2-degassing and evaporation during precipitation (cf. Lohmann, 1988). With respect to the diagenetic environment, megapores below boulders are broadly comparable to half-caves subject to changes of water supply and temperature ranging from seasons to days. As a result, the prevalent control over carbonate re-precipitation may range from CO_2-degassing to evaporation (cf. McDermott et al., 2006).

6.2.3. Shift pattern 3

This pattern, recognized in a U/Th-dated aragonite cement of Fern Pass rockslide, was tentatively interpreted to result from kinetic fractionation effects mainly from evaporation (Ostermann et al., 2007). The shift towards more positive $\delta^{13}C$ probably was enhanced by aragonite crystallization (cf. Gonzalez and Lohmann, 1988; Darling et al., 2005). Crystallization of aragonite instead of low-magnesian calcite probably was favoured by a high Mg/Ca ratio of vadose water, resulting from dissolution of dolomite, and by a high carbonate ion content because of evaporation (Ostermann et al., 2007). Furthermore, at least for shift patterns 2 and 3, respectively, biologically-induced isotope fractionations are possible, but are difficult to assess as yet.

7. Discussion

Our observations imply that meteoric lithification of rockslide deposits composed of carbonate-rich lithologies is relatively common (Fig. 9). With the few data at hand so far, no correlation is seen between rockslide event age and extent of lithification (Table 1). This may result from the complexity of the diagenetic system, including atmospheric microclimate at site, rockslide lithology and local permeability, and other factors such as slope exposition and vegetation effects. Moreover, the lithological composition down to accessories such as pyrite may influence the style of lithification. If nothing else, the different shift patterns from host rocks to cements in stable isotopes of oxygen and carbon underscore the variable character of meteoric diagenesis in the shallow portions of rockslide deposits. As mentioned above, the cements formed newly within the rockslide deposits can be used to determine a proxy age of the mass-wasting event. A methodological drawback of the U/Th approach to rockslide-event dating is that cement precipitation may continue, with interruptions perhaps, ever since emplacement of a rockslide mass. Petrographic analysis is necessary to identify the nature and suitability of cements for U/Th dating. For instance, micritic crusts are poorly suited for U/Th dating. Furthermore, early-formed cement may be of different polymorphy than later cements, such as in the Fern Pass rockslide (Ostermann et al., 2007). For the Fern Pass rockslide (Fig. 1, Table 1), a first case study using combined $^{234}U/^{230}Th$ dating, ^{36}Cl surface-exposure dating, and ^{14}C-dating had

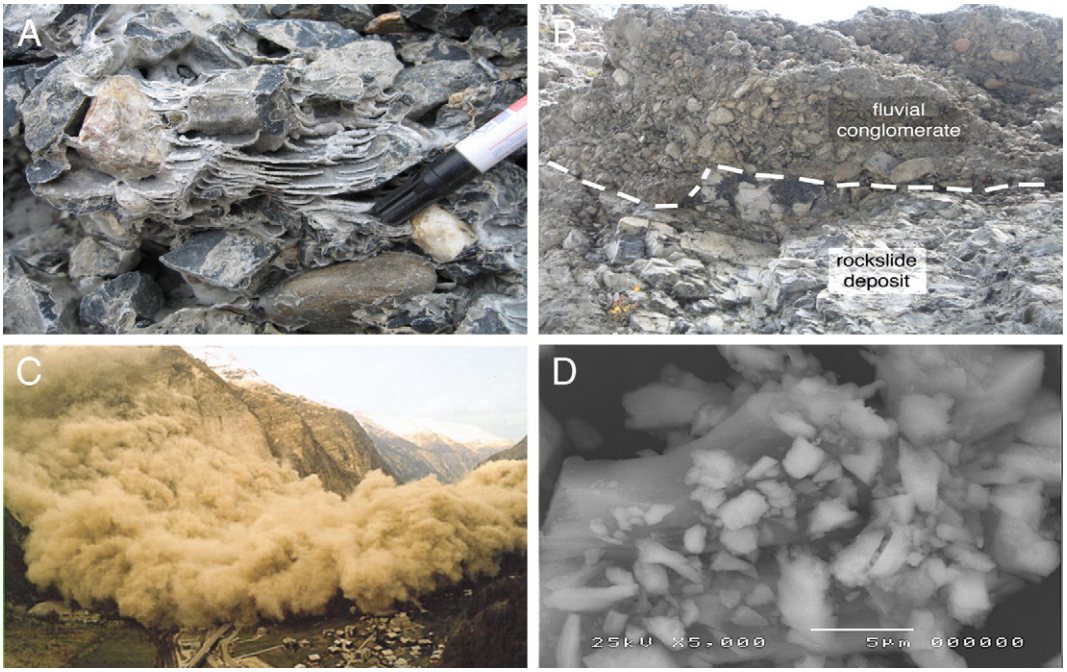

Fig. 6. A. Meteoric-vadose cements in a lithified talus slope. The talus deposits onlap onto an erosional surface incised into a rockslide mass. Rabiusa Gorge, Flims rockslide. B. Fluvial conglomerate, onlapping onto erosionally-incised rockslide mass. The conglomerate is stranded in an elevated position about 5 m above the present stream bed. Width of view about 4 m. Flims rockslide. C. Dust cloud associated with a catastrophic landslide. The photo shows the first of two events, affecting orthogneiss, in April 1991 near the village Randa, Switzerland. D. SEM image of mini-micritic (less than 1 µm in size) to siltitic rock dust produced during a large rockfall in the Dolomites, Italy (see text). (Source: www.schuepbach-kehr.ch).

demonstrated that the cement of under-boulder breccias can yield a fairly precise proxy of rockslide-event age (Ostermann et al., 2007; Prager et al., 2009). Preliminary results from $^{234}U/^{230}Th$ dating of cements from the Tschirgant rockslide (see Table 1) further underscore that most cementation proceeds immediately or soon after the mass-wasting event (Ostermann and Sanders, 2009). Another potential advantage of U/Th dating is that it can also be used to confine the rate of subsequent geomorphic change of rockslide masses, such as fluvial incision, by age-dating of cements in the 'secondary' deposits (talus slopes, fluvial deposits). Furthermore, comparatively easy and rapid sampling and small sample size render this new approach well-suited for proxy-dating rockslides in logistically difficult field situations (e. g. remote locations, little time available).

With respect to, both, the limited distribution of diagenetic minerals and the potential complexity of the diagenetic system,

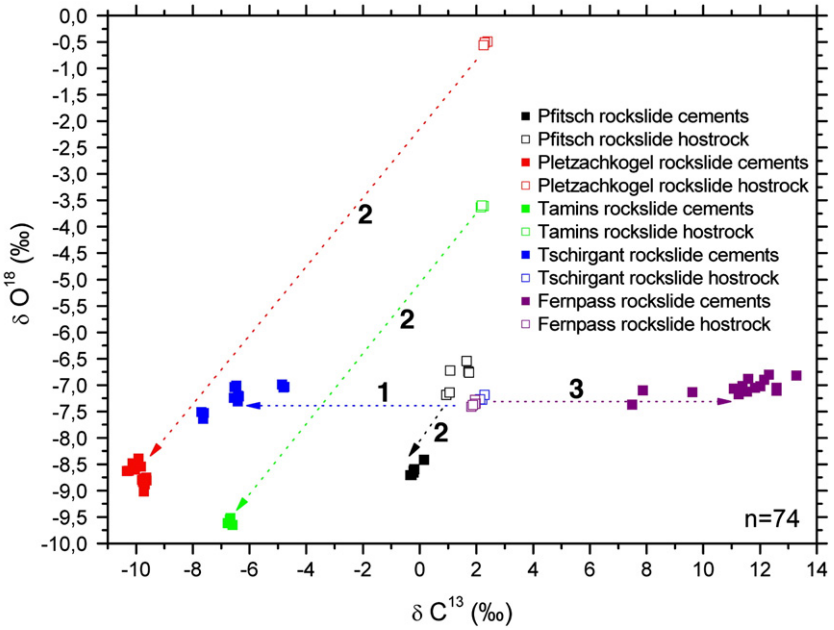

Fig. 7. Stable isotope values of oxygen and carbon of host rocks and cements from rockslides (VPDB standard). See Fig. 1 and Table 1 for locations. The shifts in isotopic composition of host rocks to cements are classified into three different types labeled 1 to 3. See text for discussion.

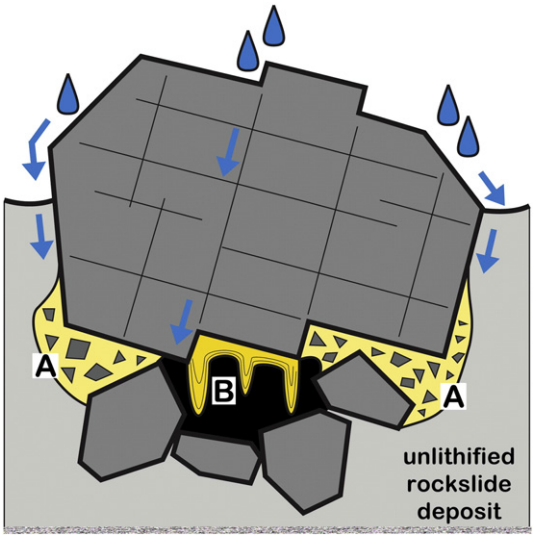

Fig. 8. Meteoric diagenetic system resulting in under-boulder breccias (A) and speleothems (B) directly below and along the underside of boulders projecting from the surface of an unlithified rockslide deposit.

rockslides may be viewed as one extreme of a spectrum of meteoric–diagenetic systems in mountainous areas. In talus-slope breccias of the Northern Calcareous Alps (Sanders et al., 2009a), for instance, stable isotope values of oxygen and carbon always show a co-variant trend towards more negative values from host rock via micritic cement to fringes of calcite spar cements. This appears consistent with meteoric diagenesis under overall steady supply of meteoric waters (Sanders et al., 2009b). The stable isotope values of cements in talus breccias, however, are difficult to interpret quantitatively in terms of palaeotemperature. This may be due to the fact that cementation of talus slopes can start a few meters to tens of meters below surface, within reach of: (a) seasonal to multi-annual temperature changes, (b) phases of relative draught and evaporation (such as summer 2003), and (c) percolation of older groundwaters from underneath into talus-slope successions (Sanders et al., 2009b). Conversely, speleothems of Alpine caves form under the comparatively most equable diagenetic conditions. Speleothems therefore are suited for reconstruction of Quaternary palaeoclimate. Even within individual speleothems, however, hiatuses may be present that must be constrained for their duration by U/Th dating (Spötl et al., 2002).

8. Conclusions

(1) Rockslide deposits composed of lithologies rich in carbonate minerals may undergo lithification in a meteoric diagenetic environment. Lithification by cement precipitation in the 'runoff shadow' below larger boulders is most widespread. More rarely, rockslides are covered by a layer of breccia, or show lithification down to their base.

(2) Diagenetic phenomena mainly include (a) diverse types of calcite cements, (b) crusts, curtains and stalactites of calcitic flowstones on the underside of boulders, (c) micritic crusts, and crusts or interstitial accumulations of micropeloidal grainstone, (d) lithification of cataclastic gouge that was produced during the rockslide event, and (e) development of solution porosity.

(3) Limestone-precipitating springs emerging from rockslide deposits, and cemented talus-slopes and fluvial conglomerates percolated by groundwaters emerging from rockslide masses indicate that rockslide deposits may shed waters supersaturated for calcium carbonate long after the mass-wasting event.

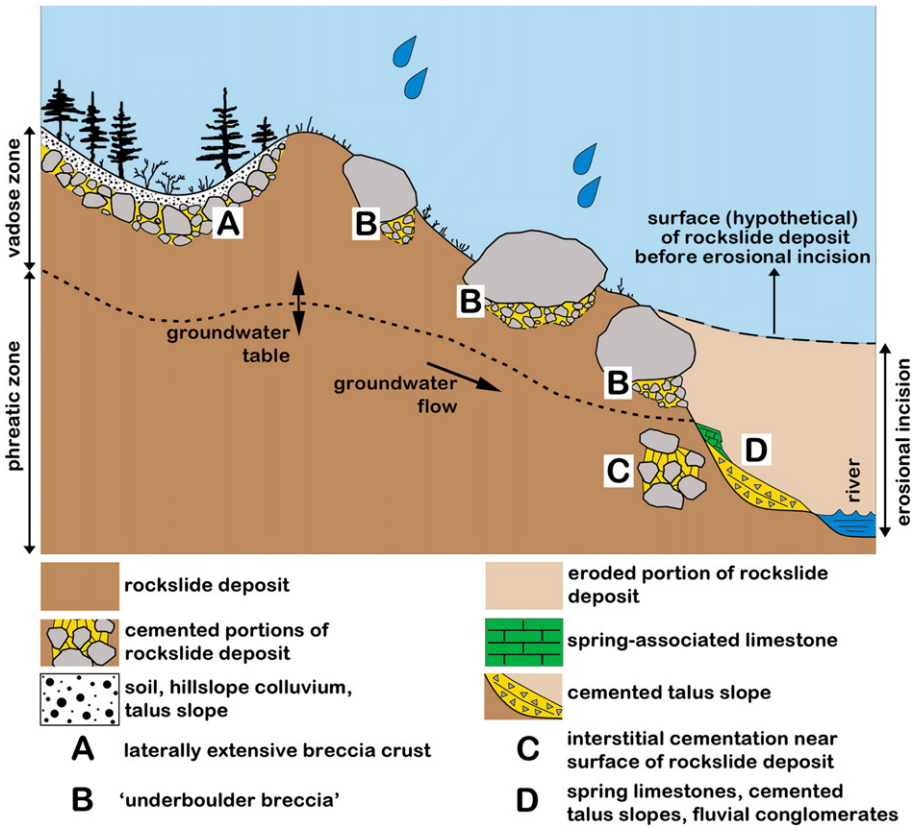

Fig. 9. Summary of diagenetic features associated with carbonate-lithic rockslide deposits. See text for description and discussion.

Acknowledgements

Financial support from project 16114-NO6 (Austrian Research Foundation), of project P20890 (Austrian Research Foundation), and of alpS project 1.3AC is gratefully acknowledged. Andreas Saxer, Institute of Material Sciences, University of Innsbruck, is thanked for help in electron microscopical investigations. The paper gained from detailed reviews by Bill Last, University of Manitoba (Canada) and Bob Scott, Precision Stratigraphy Associates, Cleveland (USA).

References

Abele, G., 1974. Bergstürze in den Alpen. Ihre Verbreitung, Morphologie und Folgeerscheinungen. Wissenschaftliche Alpenvereinshefte 25, 1–230 München.

Alonso-Zarza, A.M., Genise, J.F., Cabrera, M.C., Mangas, J., Martín-Pérez, A., Valdeolmillos, A., Dorado-Valino, M., 2008. Megarhizoliths in Pleistocene aeolian deposits from Gran Canaria (Spain): ichnological and palaeoenvironmental significance. Palaeogeography, Palaeoclimatology, Palaeoecology 265, 39–51.

Anderson, S.P., Drever, J.I., Frost, C.D., Holden, P., 2000. Chemical weathering in the foreland of a retreating glacier. Geochimica et Cosmochimica Acta 64, 1173–1189.

Ballantyne, C.K., 2002. A general model for paraglacial landscape response. Holocene 12, 371–376.

Bathurst, R.C., 1975. Carbonate sediments and their diagenesis. Developments in Sedimentology 12. Elsevier, Amsterdam. 658 pp.

Berner, E.K., Berner, R.A., 1996. Global Environment: Water, Air, and Geochemical Cycles. Prentice-Hall, New Jersey. 376 pp.

Brandner, R., Reiter, F., Töchterle, A., 2008. Überblick zu den Ergebnissen der geologischen Vorerkundung für den Brenner-Basistunnel. Geo.Alp 5, 165–174.

Burford, E.P., Fomina, M., Gadd, G.M., 2003. Fungal involvement in bioweathering and biotransformation of rocks and minerals. Mineralogical Magazine 67, 1127–1155.

Darling, W.G., Bath, A.H., Gibson, J.J., Rozanski, K., 2005. Isotopes in water. In: Leng, M.J. (Ed.), Isotopes in Palaeoenvironmental Research. Springer, New York, pp. 1–65.

Deplazes, G., Anselmetti, F.A., Hajdas, I., 2007. Lake sediments deposited on the Flims rockslide mass: the key to date the largest mass movement in the Alps. Terra Nova 19, 252–258.

Eisbacher, G.H., Clague, J.J., 1984. Destructive mass movements in high mountains: hazard and management. Geological Survey of Canada Paper 84, 1–16.

Erismann, H.T., Abele, G., 2001. Dynamics of Rockslides and Rockfalls. Springer, New York. 316 pp.

Evans, S.G., Scarascia Mugnozza, G., Strom, A.l., Hermanns, R.L., Ischuk, A., Vinnichenko, S., 2006. Landslides from massive rock slope failure and associated phenomena. In: Evans, S.G., Scarascia Mugnozza, G., Strom, A., Hermanns, R.L. (Eds.), Landslides from Massive Rock Slope Failure. : NATO Science Series. Springer, Dordrecht, pp. 3–52.

Flügel, E., 2004. Microfacies of carbonate rocks. Springer, Berlin. 976 pp.

Folk, R.L., 1974. The natural history of crystalline calcium carbonate: effect of magnesium content and salinity. Journal of Sedimentary Petrology 44, 40–53.

Frisch, W., Gommeringer, K., Kelm, U., Popp, F., 1987. The upper Bündner Schiefer of the Tauern Window — a key to understanding Eoalpine orogenic processes in the Eastern Alps. In: Flügel, H.W., Faupl, P. (Eds.), Geodynamics of the Eastern Alps. Deuticke, Vienna, pp. 55–69.

Gilchrist, A.R., Summerfield, M.A., Cockburn, H.A.P., 1994. Landscape dissection, isostatic uplift, and the morphologic development of orogens. Geology 22, 963–966.

Gonzalez, L.A., Lohmann, K.C., 1988. Controls on mineralogy and composition of spelean carbonates: Carlsbad Caverns, New Mexico. In: James, N.P., Choquette, P.W. (Eds.), Paleokarst. Springer, New York, pp. 81–101.

Heim, A., 1932. Bergsturz und Menschenleben. Fretz and Wasmuth, Zürich. 218 pp.

Höck, V., Hoschek, G., 1980. Metamorphism of mesozoic calcareous metasediments in the Hohe Tauern, Austria. Mitteilungen der Österreichischen Geologischen Gesellschaft 71 (72), 99–118.

Hölting, B., Coldewey, W.G., 2005. Hydrogeologie. Elsevier, Amsterdam. 326 pp.

Hovius, N., Stark, C.P., 2006. Landslide-driven erosion and topographic evolution of active mountain belts. In: Evans, S.G., Scarascia-Mugnozza, G., Strom, A., Hermanns, R.L. (Eds.), Massive Rock Slope Failures. : NATO Science Series. Springer, Dordrecht, pp. 573–590.

Hsü, K.J., 1975. Catastrophic debris streams (sturzstroms) generated by rockfalls. Geological Society of America Bulletin 86, 129–140.

Imre, B., Laue, J., Springman, S. M., in press. Fractal fragmentation of rocks within sturzstroms: insight derived from physical experiments within the ETH Geotechnical Drum Centrifuge. Granular Matter.

Ivy-Ochs, S., von Poschinger, A., Synal, H.-A., Maisch, M., 2009. Surface exposure dating of the Flims landslide, Graubünden, Switzerland. Geomorphology 103, 104–112.

Jiménez-López, C., Caballero, E., Huertas, F.J., Romanek, C.S., 2001. Chemical, mineralogical, and isotope behaviour, and phase transformation during the precipitation of calcium carbonate minerals from intermediate ionic solution at 25 °C. Geochimica et Cosmochimica Acta 65, 3219–3231.

Kahle, C.F., 1977. Origin of subaerial Holocene calcareous crusts: role of algae, fungi and sparmicritisation. Sedimentology 24, 413–435.

Kilburn, C.R.J., Pasuto, A., 2003. Major risk from rapid, large-volume landslides in Europe (EU project RUNOUT). Geomorphology 54, 3–9.

Klappa, C.F., 1979. Lichen stromatolites: criterion for subaerial exposure and a mechanism for the formation of laminar calcretes (caliche). Journal of Sedimentary Petrology 49, 387–400.

Klappa, C.F., 1980. Rhizoliths in terrestrial carbonates: classification, recognition, genesis and significance. Sedimentology 27, 613–629.

Lohmann, K.C., 1988. Geochemical patterns of meteoric diagenetic systems and their application to studies of paleokarst. In: James, N.P., Choquette, P.W. (Eds.), Paleokarst. Springer, New York, pp. 58–80.

McDermott, F., Schwarcz, H., Rowe, P.J., 2006. Isotopes in speleothems. In: Leng, M.J. (Ed.), Isotopes in Palaeoenvironmental Research. Springer, New York, pp. 185–225.

McSaveney, M.J., Davies, T.R.H., 2002. Rapid rock-mass flow with dynamic fragmentation: inferences from the morphology and internal structure of rockslides and rock avalanches. NATO-ARW, Massive Rock Slope Failure: New Models for Hazard Assessment. Celano, Italy, June 16–21, 2002, pp. 1–20.

Ostermann, M., Sanders, D., 2009. Proxy-dating the Tschirgant rockslide event with the U/Th method. Geophysical Research Abstracts, 12. EGU2010-24-1, EGU General Assembly 2010, Vienna.

Ostermann, M., Sanders, D., Prager, C., Kramers, J., 2007. Aragonite and calcite cementation in 'boulder-controlled' meteoric environments on the Fern Pass rockslide (Austria): implications for radiometric age-dating of catastrophic mass movements. Facies 53, 189–208.

Patzelt, G., 2004a. Tschirgant-Haiming-Pletzachkogel. Datierte Bergsturzereignisse im Inntal und ihre talgeschichtlichen Folgen. Oral presentation, alpS Symposium Naturgefahren Management 13.10.2004, Galtür (Austria).

Patzelt, G., 2004b. Die Bergstürze vom Pletzachkogel bei Kramsach und ihre talgeschichtlichen Folgen. Oral presentation, Geokolloquium 11.03.2004, Institute of Geology and Palaeontology, University of Innsbruck.

Patzelt, G., Poscher, G., 1993. Der Tschirgant-Bergsturz. Arbeitstagung 1993 Geologische Bundesanstalt: Geologie des Oberinntaler Raumes — Schwerpunkt Blatt 144 Landeck. Exkursion D: Bemerkenswerte Geologische und Quartärgeologische Punkte im Oberinntal und aus dem äußerem Ötztal. Geologische Bundesanstalt, Vienna, pp. 206–213.

Pavoni, N., 1968. Über die Entstehung der Kiesmassen im Bergsturzgebiet von Bonaduz-Reichenau (Graubünden). Eclogae Geologicae Helvetiae 61, 494–500.

Pollet, N., Schneider, J.-L.M., 2004. Dynamic disintegration processes accompanying transport of the Holocene Flims sturzstrom (Swiss Alps). Earth and Planetary Science Letters 221, 433–448.

Prager, C., Zangerl, C., Patzelt, G., Brandner, R., 2008. Age distribution of fossil landslides in the Tyrol (Austria) and its surrounding areas. Natural Hazards and Earth System Science 8, 377–407.

Prager, C.S., Ivy-Ochs, S., Ostermann, M., Synal, H.-A., Patzelt, G., 2009. Geology and radiometric ^{14}C-, ^{36}Cl- and Th-/U-dating of the Fernpass rockslide (Tyrol, Austria). Geomorphology 103, 93–103.

Sanders, D., Ostermann, M., Kramers, J., 2009a. Quaternary carbonate-rocky talus slope successions (Eastern Alps, Austria): sedimentary facies and facies architecture. Facies 55, 345–373. doi:10.1007/s10347-008-0175-z.

Sanders, D., Ostermann, M., Kramers, J., 2009b. Meteoric diagenesis of Quaternary carbonate-rocky talus slope successions (Northern Calcareous Alps, Austria). Facies. doi:10.1007/s10347-009-0194-4 online first.

Schmid, S.M., Fügenschuh, B., Kissling, E., Schuster, R., 2004. Tectonic map and overall architecture of the Alpine orogen. Eclogae Geologicae Helvetiae 97, 93–117.

Skidmore, M., Sharp, M., Tranter, M., 2004. Kinetic isotopic fractionation during carbonate dissolution in laboratory experiments: implications for detection of microbial CO_2 signatures using d^{13}C-DIC. Geochimica et Cosmochimica Acta 68, 4309–4317.

Spötl, C., Vennemann, T.W., 2003. Continuous-flow isotope ratio mass spectrometric analysis of carbonate minerals. Rapid Communications in Mass Spectrometry 17, 1004–1006.

Spötl, C., Mangini, A., Frank, N., Eichstädter, R., Burns, S., 2002. Start of the last interglacial period at 135 ka: evidence from a high-Alpine speleothem. Geology 30, 815–818.

von Poschinger, A., 2005. Der Flimser Bergsturz als Staudamm. Bulletin für Angewandte Geologie 10, 33–47.

von Poschinger, A., Kippel, T., 2009. Alluvial deposits liquefied by the Flims rockslide. Geomorphology 103, 50–56.

von Poschinger, A., Wassmer, P., Maisch, M., 2006. The Flims rockslide: history of interpretation and new insights. In: Evans, S.G., Scarascia-Mugnozza, G., Strom, A., Hermanns, R.L. (Eds.), Massive Rock Slope Failures. : NATO Science Series. Springer, Dordrecht, pp. 341–369.

Weidinger, J.T., 1998. Case history and hazard analysis of two lake-damming landslides in the Himalayas. Journal of Asian Earth Sciences 16, 323–331.

Wright, V.P., 1989. Terrestrial stromatolites and laminar calcretes: a review. Sedimentary Geology 65, 1–13.

Wright, V.P., 1994. Paleosols in shallow marine carbonate sequences. Earth Science Reviews 35, 367–395.

Yamanaka, T., Inoue, M., Kaihotsu, I., 2004. Effects of gravel mulch on water vapor transfer above and below the soil surface. Agricultural Water Management 67, 145–155.